Noninvasive characterization of the healthy human manubrium using diffuse optical spectroscopies

Parisa Farzam[1], Claus Lindner[1], Udo M. Weigel[1,2], Maria Suarez[3], Alvaro Urbano-Ispizua[3,4,5], and Turgut Durduran[1]

[1] ICFO-Institut de Ciències Fotòniques, Mediterranean Technology Park, 08860 Castelldefels (Barcelona), Spain,
[2] Hemophotonics, S.L., Mediterranean Technology Park, 08860 Castelldefels (Barcelona), Spain,
[3] Department of Hematology, Hospital Clínic, University of Barcelona, 08036 Barcelona, Spain,
[4] Institut d'Investigacions Biomédiques August Pi i Sunyer (IDIBAPS), 08036 Barcelona, Spain,
[5] Instituto de Investigación contra la Leucemia Josep Carreras, 08021 Barcelona, Spain.

E-mail: parisa.farzam@icfo.es

Abstract. The abnormal, uncontrolled production of blood cells in the bone marrow causes hematological malignancies which are common and tend to have a poor prognosis. These types of cancers may alter the hemodynamics of bone marrow. Therefore, noninvasive methods that measure the hemodynamics in the bone marrow have a potential impact on the earlier diagnosis, more accurate prognosis, and in treatment monitoring. In adults, manubrium is one of the few sites of bone marrow that is rich in hematopoietic tissue and is also relatively superficial and accessible. To this end we have combined time resolved spectroscopy (TRS) and diffuse correlation spectroscopy (DCS) to evaluate the feasibility of the noninvasive measurement of the hemodynamics properties of the healthy manubrium in thirty-two subjects. The distribution of the optical properties (absorption and scattering) and physiological properties (hemoglobin concentration, oxygen saturation and blood flow index) of this tissue are presented as the first step towards investigating its pathology.

PACS numbers: 87.64.K-, 87.64.Cc, 87.19.U-, 42.62.Be, 87.19.xj

Keywords: bone marrow characterization, near infrared spectroscopy (NIRS), hemodynamics, diffuse correlation spectroscopy, hematological malignancies.

Submitted to: *Phys. Med. Biol.*

1. Introduction

Hematological malignancies such as leukemias, lymphomas, and multiple myelomas are common, accounting for about ∼9% of all newly diagnosed cancers (Sant et al. 2010, Rodriguez-Abreu et al. 2007) and most of them have a poor prognosis (Greenberg et al. 1997, Malcovati et al. 2007). In children and adolescents younger than twenty years, hematological malignancies are the most common type of cancer, responsible for more than 30% of all cancers (Greenberg et al. 1997, Malcovati et al. 2007).

Most of these cancers originate in the bone marrow since this tissue is the main site of blood cell formation. In the bone marrow, hematopoietic stem cells (HSCs) differentiate into blood cells: red cells, white cells, and platelets. Mutations that inappropriately activate HSC proliferation cause an uncontrolled growth of abnormal blood cells and lead to hematological malignancies. This high proliferating activity of HSCs induces angiogenesis in the bone marrow (Alexandrakis et al. 2004, Wolowiec et al. 2004, Padró et al. 2000) and increase in angiogenesis of the bone marrow has indeed been observed in patients with progression of these malignancies (Negaard et al. 2009, Mangi & Newland 2000, De Raeve et al. 2004, Vacca et al. 1994, Kini et al. 2000). It has also been shown that the degree of angiogenesis is an important prognostic factor (Bhatti et al. 2006, Kumar et al. 2004, Molica et al. 2002, Salven et al. 2000), an indicator of the disease burden, and is associated with the treatment outcome (Rajkumar et al. 2002, Sezer et al. 2001).

Therefore, it is of interest to investigate the degree of vascularization of the bone marrow which is important for better estimation of prognosis and for personalization of the therapy procedure. Measurement of angiogenesis is important for the follow up of treatment and screening during the reemission phase. In the clinical routine, the most direct and common technique of angiogenesis evaluation is histomorphological analysis of the bone marrow, basically the measurement of microvessel density. It involves a bone marrow biopsy taken from the iliac crest or the sternum. However, biopsy has several limitations: it is invasive, it has substantial inter-observer variability, and analyzes just a discrete site of the whole bone marrow (Bhutani et al. 2013). Dynamic contrast enhanced magnetic resonance imaging (DCE-MRI) is also applied to investigate the degree of vascularization. Although DCE-MRI is noninvasive and has a relatively high resolution, it is expensive and utilizes contrast agents, therefore it is not suitable for screening and repeated measurements. Another clinical technique to estimate the extent of the angiogenesis is measurement of the angiogenic biomarker levels in a blood sample (Zangar et al. 2006, Gerber & Ferrara 2003). However, the estimation of biomarkers achieved by blood extraction is not targeted to a specific tissue and angiogenesis in other organs may elevate it. Therefore, the level of angiogenesis in the bone marrow and biomarkers in the blood are not necessarily correlated (Jelkmann 2001, Bertolini et al. 2007).

In experimental studies, positron emission tomography (PET) and single photon emission computed tomography (SPECT) have also been used to measure the blood

flow in the bone often as a correlate of angiogenesis (Kahn et al. 1994, Horger & Bares 2006, McCarthy 2006). PET has also been used to image the proteins, which are implicated in the angiogenesis procedure (Beer & Schwaiger 2008). Despite the good sensitivity of these techniques, high cost measurements in addition to exposure to radioactive agents make them limited for repeated measurements. They have not been adopted for widespread clinical use.

Considering the importance of angiogenesis and the limitations of current techniques, we hypothesise that the noninvasive diffuse optical spectroscopy techniques might be useful and practical to study the hemodynamics of normal and malignant hemopoiesis as a potential correlate of increased angiogenesis and proliferation. Increased angiogenesis alters the hemodynamics of the tissue which can be correlated to optical measurements of microvascular blood flow, blood volume or oxygen saturation (Mesquita et al. 2010, Pakalniskis et al. 2011).

Furthermore, in subjects with hematological malignancies, the high proliferating activity of the hemopoietic tissue is observed due to angiogenesis in the bone marrow (Alexandrakis et al. 2004, Wolowiec et al. 2004, Padró et al. 2000). Since high proliferation may alter the hemodynamics of the tissue as well as its scattering coefficient, diffuse optics can be potentially utilized for screening purposes to detect high risk subjects. Furthermore, the degree of angiogenesis has been considered a predictive factor of response to treatment. In this sense, it could be a promising noninvasive method for categorizing the risk of the patient before the treatment. It can also be applied to monitor the changes in bone marrow hemodynamics induced by the anti-angiogenic therapies which are emerging as effective treatments against cancer (Li et al. 2008, Shinkaruk et al. 2003). Following the response to the therapy may help to personalize the therapy for each subject.

Diffuse optical spectroscopy is a noninvasive method that does not use ionizing radiation or contrast agents (Durduran et al. 2010). The device and measurements are relatively inexpensive and it is a suitable method for repeated measurements. It can be combined with other modalities such as MRI (Ntziachristos et al. 2002) for simultaneous measurements to provide complementary information.

while the bulk of diffuse optics in biomedicine was used on soft tissue, the feasibility of applying optical methods on human bone tissue have been investigated in several works (Binzoni et al. 2013, Aziz et al. 2010, Bashkatov 2006, Binzoni et al. 2002, Binzoni et al. 2006, Binzoni et al. 2003, Binzoni et al. 2011, Binzoni & Van De Ville 2011, Klasing & Zange 2003, Firbank et al. 1993, Mateus & Hargens 2012, Mateus & Hargens 2013, Näslund et al. 2006, Näslund et al. 2007, Näslund et al. 2011, Pifferi et al. 2004, Prapavat et al. 1997, Ugryumova et al. 2004, Xu et al. 2001, Zhang & Jiang 2005, Farzam et al. 2013). Furthermore, it has been demonstrated that bone is an active tissue whose hemodynamics is responsive to physiological changes such as cuff occlusion (Farzam et al. 2013).

Accessibility of the target tissue is the key concern in noninvasive diffuse optical measurements since it can mostly measure the upper ($\sim$1-5 cm) layers of tissue. In

adults hematopoietic tissue exist mostly in flat bones such as the pelvic girdle and the sternum. Manubrium, the broad, upper part of the sternum is a common site for bone marrow biopsy as it is accessible and rich in hematopoietic marrow (Gordon et al. 1976). We have identified it to be also suitable for noninvasive diffuse optical probes since it is quite superficial with no overlying muscles and is sufficiently thick for adequate probing. Therefore, we have applied diffuse optical spectroscopy to measure the hemodynamics of the healthy manubrium noninvasively by combining two diffuse optical methods; time resolved spectroscopy (TRS) (Ntziachristos et al. 1999, Torricelli et al. 2013, Svensson et al. 2007, Taroni et al. 2010) and diffuse correlation spectroscopy (DCS) (Durduran et al. 2005, Durduran et al. 2010) in a single probe. This combination enabled us to measure the concentration of oxygenated and deoxygenated hemoglobin as well as the blood flow index alongside the reduced tissue scattering coefficient. In the future, with appropriate modeling, this may enable us to calculate the rate of metabolic oxygen extraction.

By this method, we characterize the optical properties (absorption and scattering coefficients) and physiological properties (hemoglobin concentration, oxygen saturation and blood flow index) of healthy bone marrow by noninvasive measurement of thirty two healthy subjects. We also investigate the effect of the location of the probed site on the manubrium, body mass index (BMI), gender, thickness of the overlying tissue and age on the distribution of the measured parameters. Our hypothesis was that the properties of health tissue has a relatively narrow distribution which would enable us to detect the changes due to pathologies. It can be used for screening purposes in order to detect subjects with a high risk of malignancy and it is repeatable which would make it a potential tool to monitor the effect of the therapy.

2. Methods & materials

2.1. Study population and the experimental protocol

All protocols and devices were approved by the ethical committee of Hospital Clínic de Barcelona where all subjects were measured. Thirty-two healthy subjects were recruited for this study (15 females and 17 males) and each subject has signed a written informed consent. Since bone marrow properties depend on age (Griffith et al. 2013, Justesen et al. 2001), in order to have a more homogeneous group of people, an age range between 25-40 years old was defined as the inclusion criteria ‡. Adolescents are of great interest to the study of hematological malignancies due to the high prevalence in that population. However, due to ethical concerns related to informed consent of minors, we have excluded them from this preliminary study.

The subjects were requested to fill a basic health questionnaire where they were asked about their history of anemia, diabetes, lung diseases, kidney diseases,

‡ Nevertheless, two subjects near to range limits (24 and 42 years old) were measured and were included in the study population.

Table 1. Vital records of the recruited subjects: median ($1^{st} - 3^{rd}$ quartile).

	Arterial oxygen saturation (%)	Heart rate (bpm)	Systolic pressure* (mmHg)	Diastolic pressure (mmHg)
All	99 (97, 99)	74 (66, 84)	119 (114, 136)	71 (67, 76)
Females	99 (99, 99)	78 (69, 88)	117 (102, 118)	71 (68, 75)
Males	98 (97, 99)	73 (65, 80)	135 (120, 140)	72 (67, 80)

* The difference between males and females is statistically significant ($P < 0.05$).

hypertension, hyperlipidemia, atrial fibrillation, congestive heart failure, coronary artery diseases, previous myocardial infraction and smoking. Each subject reported whether they have any other diseases and their current medications. Subjects with the history of any type of malignant neoplasms or severe anemia were excluded from this study. Among all subjects, two of them were under medication for thyroiditis and one subject for asthma. These medications do not have any known impact on the bone marrow hemodynamics, therefore, we have included these subjects in the study. There were also three smokers among the subjects who were included in the data, which may affect the systemic hemodynamics. In Table A1, Table A2, and Table A3 they are labeled by a star sign. Furthermore, before (in a few cases, after) the optical measurement, the vital signs (heart rate, arterial blood pressure and arterial oxygen saturation) were measured to assure that the subject is in normal health condition and to explore any correlations with the results. The vital records are summarized in Table 1 and the physical characteristics in Table 2. Body mass index (BMI) is calculated by dividing the weight [kg] by square of the height [m]. The thickness of the tissue overlying manubrium skin was estimated by the caliper skinfold measurement. These two parameters are highlighted since they may effect the optical measurement.

Table 2. Physical characteristics of the recruited subjects: median ($1^{st} - 3^{rd}$ quartile).

	Age* (year)	Weight* (kg)	Height* (cm)	BMI* (kg/m^2)	Skinfold/2 (mm)
All	30 (27, 33)	74 (58, 84)	172 (164, 180)	23.3 (21.6,26.7)	4.7 (3.9, 6.2)
Females	29 (27, 30)	58 (53, 62)	163 (160, 169)	21.4 (20.7,23.4)	4.4 (3.6, 4.8)
Males	32 (27, 35)	79 (73, 86)	180 (177, 183)	24.5 (23.3,26.8)	5.1 (4.3, 7.0)

* Difference between males and females is statistically significant ($P < 0.05$).

For the measurements, the subjects were asked to sit comfortably on a chair with the head tilted back. A hematologist with experience in bone marrow biopsies located the manubrium and marked the outside borders to guide the positioning of the optical probe. The height of each manubrium was divided into four regions from top to bottom (neck to breast) labeled as one to four. The markings and the probe placement are illustrated in Figure 1. On each location, three measurements were performed.

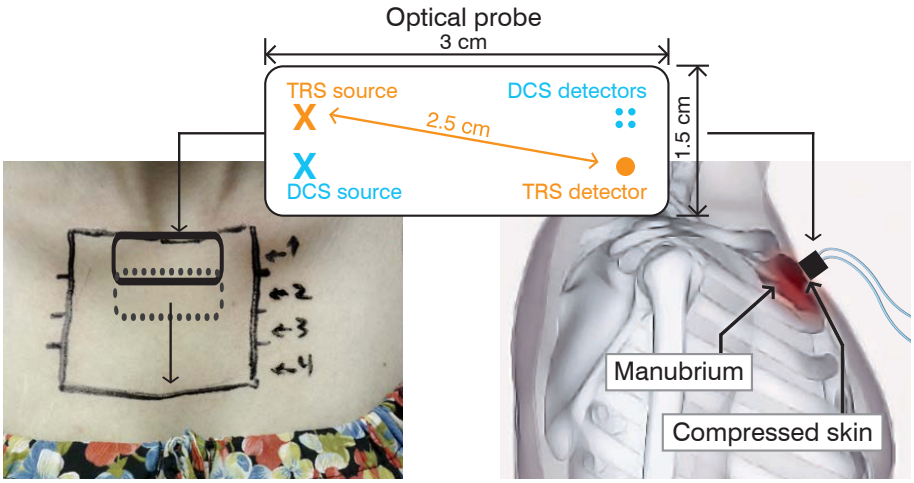

Figure 1. (Left) The photograph of the manubrium of a female subject. The lines show the outer border of the bone marked by a hematologist. The height is measured and divided into four regions. The dashed/solid rectangles indicate the approximate probe positions. (Right) The location of sternum in the upper part of the skeleton. The drawing is adopted from the Wikimedia Commons.† The probe is pressed to the manubrium so that the skin on the contact area is compressed. (Top) The schematic of the probe with one source and one detector for TRS (source-detector separation = 2.5 cm) and one source and four detectors for the DCS device (source-detector separation = 2.5 cm).

2.2. The device and the probe

The custom-built TRS instrument consists of three pulsed lasers (Becker & Hickl, Berlin, BHLP-700) emitting at 687, 785 and 830 nm with pulse widths of 400, 350, and 450 pico-seconds respectively for each wavelength and a repetition rate of 50 MHz. The pulses are sent to the tissue using a 10 meter long fiber with a 90° bent tip and a core diameter of 62.5 μm ($NA = 0.275$). The diffuse light was collected by a custom made bundle that consists of 54 graded index multimode fibers and delivered to a hybrid photo multiplier tube (PMT, Becker & Hickl,Berlin, HPM-100-50). A standard time-correlated single photon counting (TCSPC) setup (Becker & Hickl, Berlin, Simple-Tau 130) is used to record and store the distribution of the time of flights of the diffuse photons (Ntziachristos et al. 1999).

The DCS part of the setup uses a single longitudinal mode laser as the source (CrystaLaser, Reno, NV, USA) at 785 nm whose coherence length (> 10 m) is much longer than the distribution of typical photon path lengths. The laser light is delivered to the tissue through a multimode fiber with a core diameter of 200 μm ($NA = 0.22$). Since DCS uses single mode fibers of 5.6 μm core diameters for collection which limits the detected photon count rate, we bundle four fibers together to improve the signal-to-noise ratio. Four photon counting avalanche photodiodes are used as detectors (Excelitas,

† Retrieved December 30, 2013, from "http://commons.wikimedia.org/wiki/File:Manubrium_lateral.png"

Quebec, Canada) whose output is fed to a digital correlator (Correlator.com, New Jersey, USA) to obtain the autocorrelation functions. Details of the DCS system is discussed in various reviews (Durduran et al. 2010, Yu 2012).

Both time resolved spectroscopy (TRS) and diffuse correlation spectroscopy (DCS) are combined in a single probe as illustrated in Figure 1. For both, TRS and DCS, we use a source-detector separation of 25 mm. For each location there were three acquisitions with an averaging time of three seconds for DCS and three seconds per wavelength for TRS amounting to approximately ten seconds per measurement.

2.3. Data analysis

2.3.1. Theory and calculations of TRS measurement The experimental data is fitted with a solution of the diffusion approximation for a semi-infinite homogeneous medium (Patterson et al. 1989) to extract the values of the reduced scattering (μ_s') and absorption (μ_a) coefficients for each wavelength.

In this process the theoretical curve is convoluted with the instrument response function. The fitting range includes the points with a number of counts higher than 80% of the peak value on the rising edge of the curve and 1% on the tail. The fitting was performed by "fminsearch" function of Matlab (Mathworks Inc, Massachusetts, USA).

The measured absorption coefficients ($\mu_a(\lambda\ )$) are related to the different tissue chromophores as $\mu_a(\lambda) = \sum_i^{nc} \epsilon_i(\lambda) c_i$. The sum is over the different tissue chromophores. Here we have assumed only water, oxy- and deoxy-hemoglobin as chromophores ($nc = 3$). $\epsilon_i(\lambda)$ is the wavelength-dependent extinction coefficient of the i_{th} chromophore obtained from the literature (Prahl n.d.) and c_i is the concentration of the i_{th} chromophore. The water concentration in the bone was assumed to be 30% (White et al. 1987) and oxy- and deoxy-hemoglobin concentrations were measured (c_{HbO_2}, c_{Hb}). The total hemoglobin concentration (THC) was calculated as the sum of oxy- and deoxy-hemoglobin, i.e. $THC = c_{HbO_2} + c_{Hb}$ and blood oxygen saturation, $SO_2 = \frac{c_{HbO_2}}{THC} \times 100$ was also calculated and reported.

2.3.2. Theory and calculations of DCS measurement DCS measures the temporal speckle fluctuations of the scattered light, that is sensitive to the motions of scatterers such as red blood cells which in turn could be used to estimate microvascular blood flow (Boas et al. 1995, Durduran et al. 2010). The dynamics of the medium can be determined by the measurement of the intensity autocorrelation from which the electric field autocorrelation function can be derived. The semi-infinite homogeneous medium solution to the correlation diffusion equation was employed to fit to the measured autocorrelation curves, for a blood flow index (BFI) (Durduran et al. 2010).

For the fitting we have used the "fminsearch" function of Matlab (Mathworks Inc., Natick, MA, USA). The measured μ_a and μ_s' by TRS for each subject (averaged over all locations and acquisitions) was introduced as an input for DCS analysis.

2.4. Statistical analysis

As a first step, we have explored the measured parameters to check if the data has a normal distribution. The normality was tested using a two sided "Shapiro Wilk" test. We have cross-checked the results of "Shapiro Wilk" test by quantile-quantile plots. Both tests were in agreement with each other.

For each measured parameter (μ_a, μ_s', THC, blood flow index, and oxygen saturation) the median as well as $1^{st} - 3^{rd}$ quartile values are reported.

To examine the correlation between different measured parameters we have fitted a linear mixed effects (LME) model (Pinheiro & Bates 2000, Winter 2013) using packages "lme4" (Bates et al. 2013) and "lme4test" (Kuznetsova et al. 2013) in R (open source statistical computing language (R Core Team 2013)). This method was utilized since it does not have a strict normality assumption (Pinheiro & Bates 2000). In all the analysis, the normality of the residuals were examined visually and no obvious deviations from normality were revealed. We rejected results in which the full model did not differ signicantly from the null model.

To test the dependency of the optical parameters on the location of the probe we have fitted an LME with the location as the fixed effect. The subject was considered as the random effect in this model. In this analysis, the first location is considered as the reference.

The correlation between measured physiological parameters (blood flow, blood volume and oxygen saturation) were also investigated by LME. Since we have observed a dependency of measured parameters on the location of probe, here both location and measured parameter were fixed effects and subject was the random effect.

We have applied LME model to study the effect of BMI, skinfold value, and age of the subjects on the measured physiological parameters. In these models the parameter under the investigation (BMI, skinfold, age) and the location of the measurement were the fixed effects and the subject was the random effect.

Furthermore, the effect of gender on the measured parameters was examined. Since we have observed a difference between BMI of males and females and a significant effect of BMI on the measured parameters, we have considered gender, BMI and location as the fixed effects. Here the subject was the random effect.

At the end, in order to investigate the effect of our assumptions on our results, we have calculated the hemodynamic parameters (THC and oxygen saturation) assuming different concentrations of chromophores (bone mineral and lipid). The difference between distribution of physical parameters under different assumptions was investigated by student's t-test. Throughout this study, "p-values" less than 0.05 were considered statistically significant to reject the null hypothesis.

3. Results

3.1. The distribution of the measured optical and physiological parameters

Figure 2 shows the histogram of the distribution of the measured parameters for all subjects over four locations on the sternum. The Shapiro-Wilk test shows that the values of measured THC and blood oxygen saturation are normally distributed while the blood flow index does not have a normal distribution. For all three wavelengths μ_a values are normally distributed and μ_s' distributions were not normal.

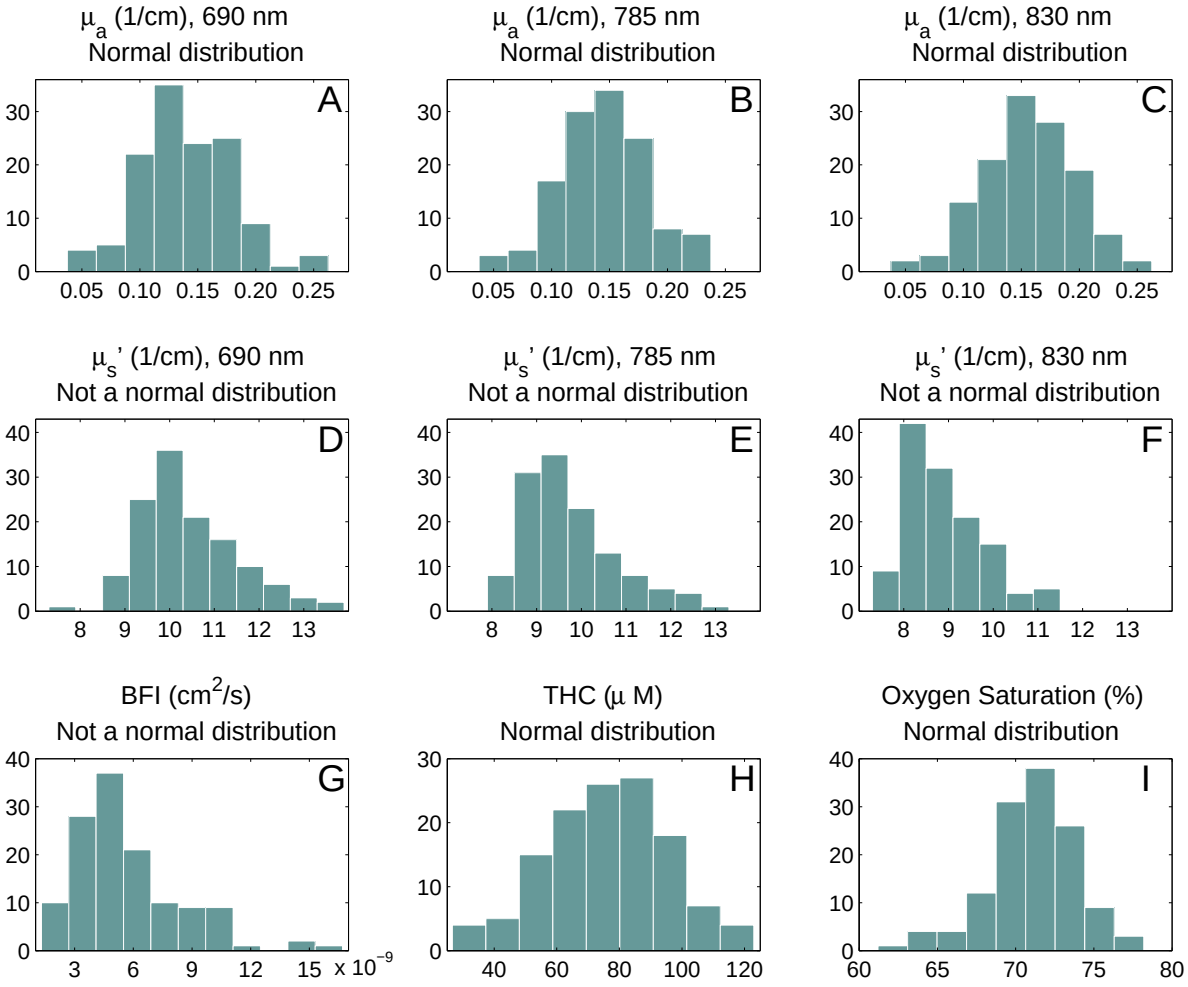

Figure 2. The distribution of the measured hemodynamics over four locations on the sternum for all subjects. (A-C) In each wavelength μ_a has a normal distribution. (D-F) μ_s' does not have a normal distribution in any wavelength. (G) The blood flow index is not normally distributed. (H) Total hemoglobin concentration values are normally distributed. (I) Blood oxygen saturation values are normally distributed.

The summary of all the measured optical and physiological parameters are listed in Table 3. Each parameter is presented with its median and $1^{st} - 3^{rd}$ quartile range. For completeness, the data from each individual subject is presented in Appendix 1; Table A1, Table A2 and Table A3.

Table 3. Median and inter-quartile range values for the measured parameters.

	$\lambda = 690$ nm	$\lambda = 785$ nm	$\lambda = 830$ nm
μ_a (cm^{-1})	0.14 (0.12, 0.17)	0.15 (0.12, 0.17)	0.16 (0.13, 0.18)
μ_s' (cm^{-1})	10.1 (9.7, 10.9)	9.6 (9.0, 10.2)	8.7 (8.3, 9.5)
BFI (cm^2/s)	5.0×10^{-9} (4.2×10^{-9}, 7.4×10^{-9})		
THC (μM)	77.3 (62.2, 88.6)		
Oxygen saturation (%)	71.1 (69.5, 72.3)		

3.2. The sensitivity of the measurements to the location of the probe

The distribution of the measured physiological parameters over four measured locations are illustrated in Figure 3. The intercept is the LME fitted value for the location 1 and the slope shows the change in comparison to the location 1. In Table 4 the fitted value for the first location (intercept) and the slope (changes between two consecutive locations) are listed. In all cases, both the intercept and the slope are statistically significantly different ($P < 0.05$) from zero indicating a clear yet small dependence on the location.

Table 4. The fitted value for the first location (intercept) and the slope (changes between two consecutive locations). All cases show statistically significant changes ($P < 0.05$).

	$\lambda = 690$ nm	$\lambda = 785$ nm	$\lambda = 830$ nm
μ_a (cm^{-1})	0.151 (- 0.005)	0.154 (- 0.003)	0.165 (- 0.004)
μ_s' (cm^{-1})	11.0 (-0.2)	10.2 (- 0.2)	9.4 (- 0.2)
BFI (cm^2/s)	4.8×10^{-9} ($+ 0.3\times10^{-9}$)		
THC (μM)	80.4 (- 1.8)		
Oxygen saturation (%)	69.8 (+ 0.4)		

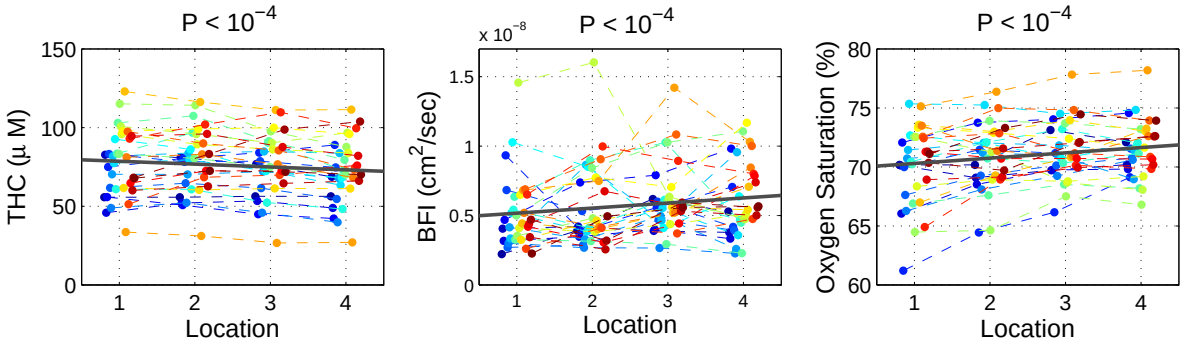

Figure 3. Measured parameters for 32 subjects over 4 locations on manubrium. For clarity points are moved slightly along the x-axis ("dodging"). (Left) total hemoglobin concentration (μM). (Middle) blood flow index (cm^2/sec). (Right) oxygen saturation (%).

3.3. Correlation between the measured parameters

Figure 4 demonstrates how measured physiological parameters are correlated with each other on a specific location (location 3). From this point on, the location is considered as a fixed effect in the LME fitting (see Section 2.4) leading to a positive correlation between blood flow and total hemoglobin concentration ($P = 0.01$) yet the changes are small. Moreover, the subjects with higher blood flow have a higher blood oxygen saturation ($P < 10^{-4}$). The correlation between total hemoglobin concentration and oxygen saturation is not statistically significant ($P = 0.1$). In all the subsequent plots and analysis, we will focus on one of the central locations, location 3.

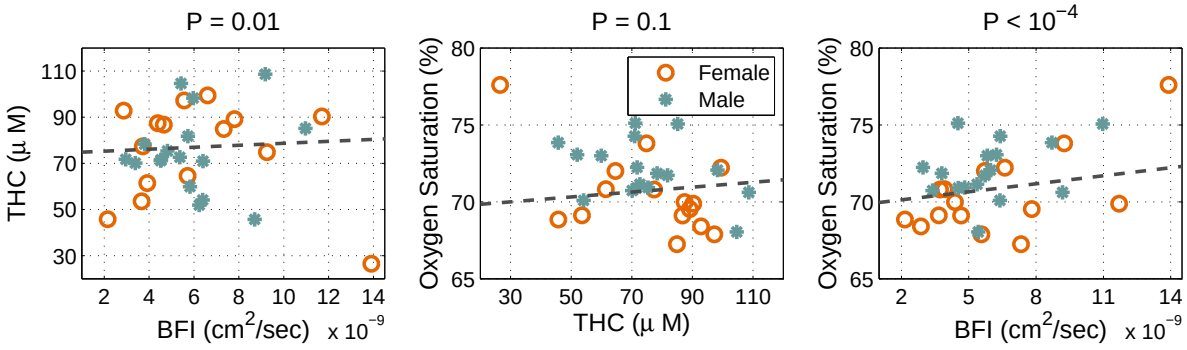

Figure 4. Correlation between the measured physiological parameters. The plot represents measured values and the fitted line for the location 3 of the manubrium. (Left) Subjects with higher blood flow have higher total hemoglobin concentration. (Middle) Total hemoglobin concentration and oxygen saturation are not correlated. (Right) Subjects with higher blood flow have higher oxygen saturation.

3.4. The sensitivity of the measurement to the physical condition of the subjects

For each subject we have performed the skinfold measurement on the manubrium area to estimate the thickness of overlying tissue. As it is shown in Figure 5 there is a positive correlation between BMI and skin thickness, as may be expected, since the skinfold measurement includes the overlying adipose layer ($P < 10^{-4}$).

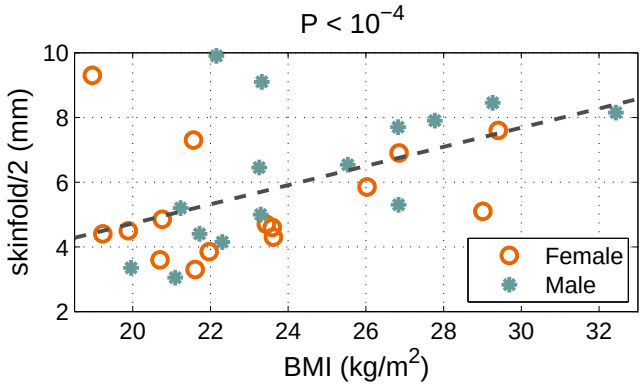

Figure 5. There is a positive correlation between BMI and skinfold value on the manubrium ($P < 10^{-4}$).

Figure 6 compares the measured physiological parameters (THC, BFI, and oxygen saturation) with the thickness of overlying tissue (skinfold value) in a central location of the manubrium (location 3). None of the physiological parameters have shown a significant correlation to the skinfold value.

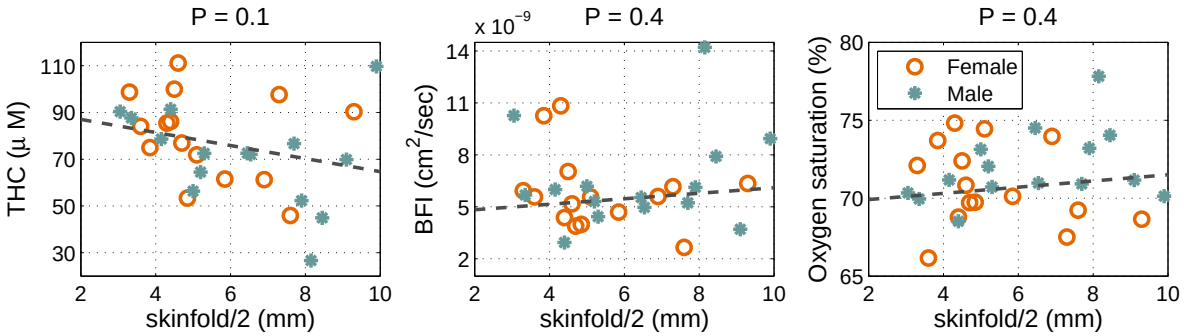

Figure 6. There is no significant correlation between the skinfold value and (Left) total hemoglobin concentration. (Middle) blood flow index. (Right) oxygen saturation. The plot represents measured values and the fitted line for the location 3 of the manubrium.

Figure 7 demonstrates that the measured THC and oxygen saturation are dependent on the BMI of the subject. There is a negative correlation between BMI and THC ($P < 10^{-4}$) and there is a positive correlation between BMI and the oxygen saturation ($P = 0.003$). Despite the correlations observed for the total hemoglobin concentration and the oxygen saturation, no correlation was observed between BMI and blood flow index. The plot represents measured values and the fitted line for the location 3 of the manubrium.

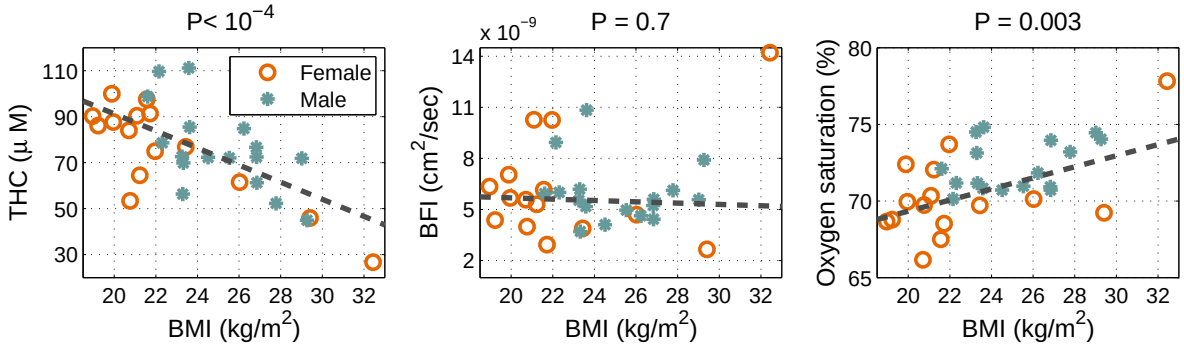

Figure 7. (Left) BMI has a negative correlation with total hemoglobin concentration ($P < 10^{-4}$). (Middle) There is no significant correlation between BMI and the blood flow index ($P = 0.7$). (Right) BMI has a linear correlation with the oxygen saturation ($P = 0.003$). The plot represents measured values and the fitted line for the location 3 of the manubrium.

3.5. The dependency of the physiological parameters on gender

To test the dependency of the physiological parameters on the gender, we have fitted an LME model to the data. If gender is considered as the only fixed effect then the oxygen saturation in the males is 2% higher than in the females. Since BMI is an influential

parameter, and two genders have signicantly different BMIs (Table 2), both BMI and gender were considered as the fixed effects. In this case there is no significant difference between genders on any of the measured parameters (P = 0.4).

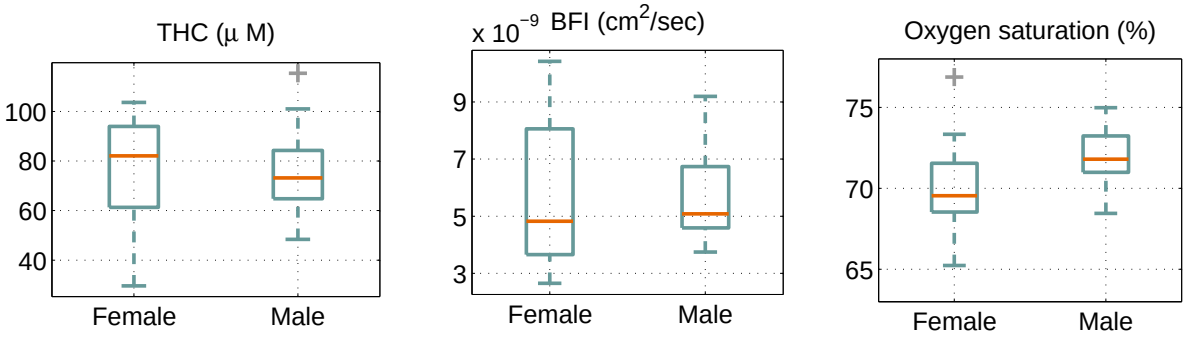

Figure 8. The distribution of the measured physiological parameters by gender. (Left) total hemoglobin concentration, (Middle) blood flow index (BFI), (Right) blood oxygen saturation.

3.6. The dependency of the physiological parameters on age

We have chosen the subjects from a controlled range of age (24-42 years) to try to avoid the dependency of the measurement on the age of subjects. Figure 9 demonstrates that in the collected range of ages the measure physiological parameters do not depend on the age.

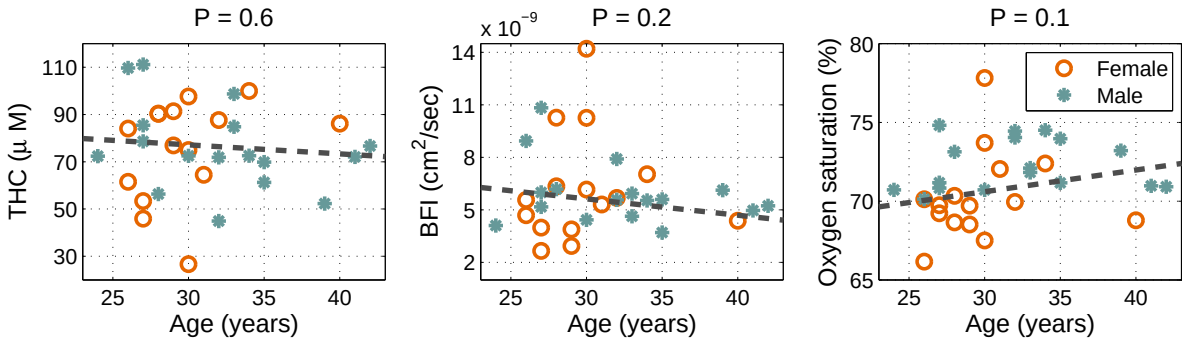

Figure 9. There is no significant correlation between age and (Left) total hemoglobin concentration. (Middle) blood flow index. (Right) oxygen saturation. The plot represents measured values and the fitted line for the location 3 of the manubrium.

4. Discussion

In this work, we have studied the optical and physiological properties of the healthy manubrium bone as a site indicative of the red bone marrow hemodynamics in the body. We first discuss the quality of the measurements and whether the bone marrow is the main contributor to our optical signal. Then the distribution of the measured parameters on the healthy subjects is reviewed, the sensitivity of measured parameters to the location of probe on the manubrium is discussed and the correlation between

measured physiological parameters and characteristics of subjects such as BMI, skinfold value, age and gender are discussed.

The quality of the measurements and the probed tissue volume: In each measurement, an experienced hematologist located the manubrium and guided the placement of the probe. We were able to obtain data with sufficient signal-to-noise ratio from each measurement and the fitting for both DCS and TRS device had good quality indicating that the data fits the model well and there are no systematic deviations from the model. The source-detector separations were 25 mm for both modalities.

Manubrium is a superficial tissue that does not have any overlying muscle. Its average size is 50×50 mm^2 with thickness of ≈ 11.2 mm in females and ≈ 12.6 mm in males (Selthofer et al. 2006). The manubrium is not homogeneous in thickness and these numbers were measured on two points which represent the average of extreme values (thinnest and thickest part) of the manubrium. The thickness of combined skin and the manubrium is approximately 15.6 mm and 17.7 mm respectively for females and males. On average, the depth of optical penetration with our probe is greater than the thickness of the skin and less than the combined thickness of the skin and the manubrium. However it has been reported that manubrium in the thinnest part can be less than 10 mm (Gao-ju & Qing 2011, Xiu et al. 2012). To study this point we have simulated a medium (data not shown) with similar optical properties as manubrium and we have calculated the probability of detecting a photon which has penetrated a certain depth. We observe that less than 20% of detected photons had penetrated more than 1 cm assuming a homogeneous medium. However, due to the presence of thymus and large vessels below the manubrium we expect a lower contribution to our signals. Finally, change of μ_a between 2 consecutive locations, on average, is $\sim$3% (Table 4). We know that manubrium is thickest on the location 1 and narrower in locations 2-3, and again gets thicker in location 4. However, μ_a drops unidirectional from location 1 to 4. This suggests that in thinner parts we are not probing different tissue. This small yet significant location dependency is not due to variation in thickness. Therefore, it is a reasonable assumption to consider manubrium bone and its rich red bone-marrow content as the the dominant contributor to our signal.

Furthermore, to double check this assumption, for one subject, we have located the manubrium by an ultrasound and compared its dimensions to the average which was well within the average and to the borders defined by the hematologist. Two sets of data were taken, one based on the hematologist's assumptions and one guided by the ultrasound. The measured parameters in both cases did not show any significant differences (data not shown).

The distribution of the measured parameters: Bone is a relatively understudied organ for diffuse optics. It is often considered a nuisance, for example, when dealing with the measurements on the adult head (Durduran & Yodh 2014, Torricelli et al. 2013). However, a few groups have measured *in vivo* human bones to investigate absolute values

of μ_a and μ_s' (Pifferi et al. 2004, Xu et al. 2001, Farzam et al. 2013). The first study (Pifferi et al. 2004) has investigated the calcaneus bone ($\mu_a \approx 0.07$ and $\mu_s' \approx 14$ (cm^{-1}) for $\lambda = 785$ nm), and the second one (Xu et al. 2001) has measured the finger bone ($\mu_a \approx 0.20 - 0.25$ and $\mu_s' \approx 20 - 25$ (cm^{-1}) for $\lambda = 785$ nm). The last study (Farzam et al. 2013) has investigated the patella bone and they have reported $\mu_a \approx 0.035$ and $\mu_s' \approx 5.4$ (cm^{-1}) for $\lambda = 785$ nm. The reported μ_a, μ_s' in this study ($\mu_a \approx 0.15$ and $\mu_s' \approx 9.6$ (cm^{-1}) for $\lambda = 785$ nm) is in the range of the previous measurements but, we note that, the reported values from different studies cover a wide range. This may be due to differences in the tissue and bone structure in different sites and also the limited number of subjects in all studies.

Absorption coefficient and the physiological parameters derived from it (total hemoglobin concentration and oxygen saturation) have normal distributions. The median of THC value is 77.3 (μM) with the quartile range (QR) of 62.2-88.6 (μM). This value is much higher than the measured THC in patella bone ($\approx 18\mu M$) (Farzam et al. 2013). It can be explained by the higher red marrow cellularity in manubrium in comparison to the patella. Since hematopoietic tissue is physiologically more active compared to compact bone, it has a wider vasculature niche, i.e. is better perfused, to provide it with oxygen and nutrition. Higher vascular level of the manubrium suggests higher THC values and our measurements confirm it. The median oxygen saturation of all subjects is 71.1% (QR:69.5-72.3%) which is in the range of the oxygen saturation observed in the patella.

In contradiction to other parameters, the blood flow index does not show a normal distribution. This might be partially due to the relatively higher standard deviation of the absolute values from the DCS measurements or it may reflect the underlying physiology. We note that an overwhelming majority of the DCS studies, to date, have reported relative changes in blood flow with respect to a reference tissue or time point since the DCS results depend on the optical parameters of the tissue (Durduran & Yodh 2014, Mesquita et al. 2011, Durduran et al. 2010, Irwin et al. 2011). Our study stands out in this aspect since we use the TRS values for more accurate analysis of the DCS data. However, DCS is a highly sensitive measurement of the local blood flow, and, in soft tissues, this may depend on the probe pressure as was documented for the scalp Mesquita et al. (2013). We discuss this point further in the following paragraphs.

The knowledge about the range of the measured physiological parameters and their distribution enables us to define the healthy range to detect the subjects with high risk of hematological malignancies since a high proliferating activity of the hemopoietic tissue due to malignancy is related to angiogenesis (Alexandrakis et al. 2004, Wolowiec et al. 2004, Padró et al. 2000) and can cause high hemoglobin concentration or high blood flow in the bone marrow. This will be the topic of our future studies.

One shortcoming of our study is that we have assumed water, oxy-, and deoxy-hemoglobin as the only major absorbers due the limited number of wavelengths that were utilized. In fact, the water concentration was kept constant at 30% (White et al. 1987). Other significant absorbers in manubrium could be the lipids and the bone mineral

which were not considered in the above analysis. Errors in these estimates could effect the derived parameters such as the total hemoglobin concentration and the blood oxygen saturation.

To further investigate this point, we have calculated the hemoglobin concentrations for different assumptions of lipid and bone concentrations started from 5%, since assuming lower than 5% of lipid and bone does not practically change any of measured values. It has been shown (Griffith et al. 2013, Griffith et al. 2005) that bone marrow is made up of $\sim 30-40\%$ fat in the people with same age range as the subjects of this study. To study more extreme cases we have assumed 50% fat for the upper limit of the assumed fat concentration. Previous, studies on sternum have demonstrated that it has less than 14% bone mineral in healthy subjects (Arbabi 2009). Here we have assumed 20% as the upper range for the mineral concentration. The spectra of the lipid and the bone mineral were obtained from Ref. Van Veen et al. (2004) and Ref. Pifferi et al. (2004) respectively.

Table 5. The effect of assuming different concentrations of lipid and bone mineral on total hemoglobin concentration and blood oxygen saturation calculations.

	THC (μM)	Oxygen saturation (%)
Only water	77.3 (62.2, 88.6)	71.1 (69.5, 72.3)
Lipid 5%	77.1 (62.4, 88.5)	71.1 (69.4, 72.3)
Lipid 50%	75.7 (60.7, 87.1)	70.7 (69.0, 72.0)
Bone 5%	76.4 (61.3, 87.7)	71.4 (69.8, 72.6)
Bone 20%	73.6 (58.6, 85.0)	72.2 (70.7, 73.6)

Manubrium is mostly red marrow with a soft and spongy inner structure which suggests that it has a low concentration of bone mineral (Gordon et al. 1976, Arbabi 2009). However, even assumption of 20% bone mineral does not introduce a significant difference in the distribution of measured hemoglobin concentration ($P = 0.4$) and the averaged change in the oxygen saturation is less than 1.5%. In a study on an elder group of people (67–101 years) who are expected to have a higher fat content (fat content increases by aging), the average percentage of measured fat was 50% (Griffith et al. 2005). It demonstrates that assuming 50% as the upper limit is a reasonable assumption. Even the extreme assumption of 50% for fat content does not change significantly the distribution of measured hemoglobin concentration ($P = 0.7$) and oxygen saturation ($P = 0.5$). Table 5 demonstrates that assumptions of extreme values for bone or mineral concentration changes the measured THC in the range of 73.6-77.3 μM and oxygen saturation between 70.7-72.2%. For all assumed concentrations of lipid and bone,both THC and blood oxygen saturation are normally distributed.

The dependency of the measured parameters on the probe location: As it was mentioned the height of manubrium was divided to four locations and we measured the locations from top to bottom (location 1-4). The measured parameters have a slight change over

the first to last location of probe (see Table 4). Although the change is statistically significant, it is less than 5% (between two locations).

Since all the measurements were done in the same order, to test the repeatability of the measurements when the order is changed, we have repeated the measurements on two subjects. Here, we measured the manubrium four times per subject; two measurements top to bottom and two measurements bottom to up. The results indicate that the measurement order is not an effective parameter (Figure 10).

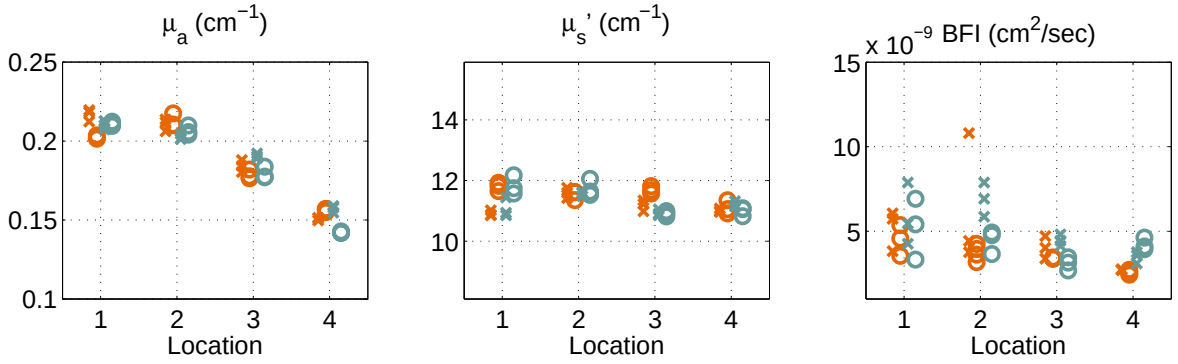

Figure 10. Four measurements on four locations. Crosses are measurements from top to bottom and circles are representing measurements from bottom to top. Orange is the first measurement and blue the second time. The plot demonstrate the independency of the results on the order of measurements. (Left) Absorption coefficient. (Middle) Scattering coefficient. (Right) Blood flow index.

Small dependency of the measured value on the location of probe suggests that in the next series of measurement on the healthy or malignant manubrium very precise locating of probe is not necessary. We can approximately put the probe on the center of manubrium. Since the measured values do not depend on the order of measurement, we can relocate the probe couple of times to have an average value of all positions near to center of manubrium for each subject.

Correlations between the measured parameters: Figure 4 demonstrates the correlation between measured physiological parameters. Oxygen saturation and hemoglobin concentration increases (however the change is small) when the blood flow increases. These are within expectations. The lack of or small correlation between parameters reflects the differences in the baseline metabolism of the subjects. It strengthens our motivation to use hybrid diffuse optics for this study.

The sensitivity of the measurement on the overlying tissue and the pressure on it: In this measurement the skin-fat tissue is a non-desirable volume that is located between the optical probe and the manubrium. We try to minimize the partial volume effect of this superficial tissue. The partial volume effect problem in this study is similar to the brain measurements with less complication, because in the brain measurements

there are several a non-desirable layers (skin-fat, skull and cerebrospinal fluid) some of which (skull) are not directly accessible. Despite all these layers the penetration of near infrared light in the brain is well-validated (Durduran & Yodh 2014). Mesquita et al. (2013) demonstrated that the application of pressure to the optical probe (which is transmitted to the tissue in contact with the probe) would alter the partial volume effect contributions from the scalp and minimize them at the highest pressures. With the goal of minimizing the partial volume effect we have have applied high (but still comfortable) probe pressures. The target tissue in this study is a bone. While the probe pressure compresses the overlying tissue and alters the hemodynamics, due to the rigid structure of the manubrium we do not expect its hemodynamics to be affected by pressure. Furthermore, we have tested the effect of probe pressure on the manubrium by putting a load sensor between the manubrium and optical probe (Figure 11).

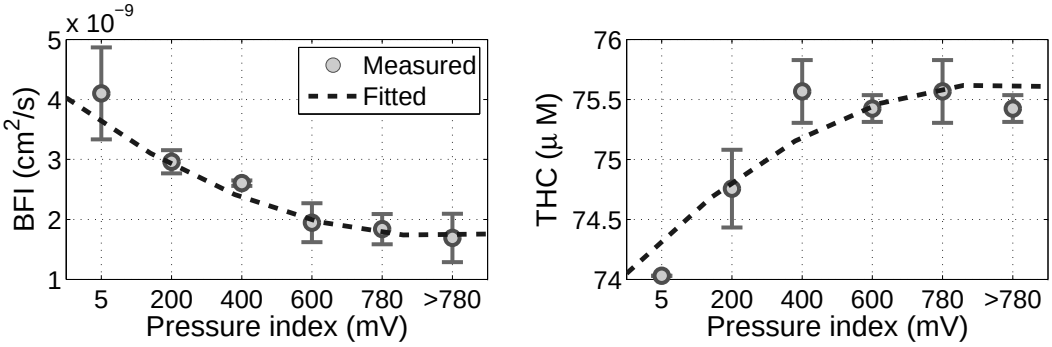

Figure 11. The effect of probe pressure on the measurement of (Left) total hemoglobin concentration and (Right) blood flow index. In the low pressure regime the measured values are sensitive to the pressure increases until the pressure reaches to a threshold value. After the threshold, the increase in probe pressure does not change the measured THC or blood flow index.

In the low pressure condition, an increase in pressure led to a higher THC (lower BFI) up to a certain pressure threshold. The increased probe pressure "squeezes out" the superficial blood and, therefore, we probe a larger portion of the manubrium which has a higher THC than overlying tissue (skin and fat) and lower blood flow. This, in turn, leads to the observed changes. After reaching the threshold, there is a plateau and pressure change does not affect the measured parameters. Therefore, in the measurement of subjects we kept the pressure at the highest possible, comfortable amount. Considering our probe design, fibers tips protrude out of the probe surface, presumably such a pressure compresses the overlying tissue on the measured area (Figure 1) and minimizes the skin effect. A future probe may include a calibrated load sensor to equalize this effect between subjects.

The sensitivity of the measurement to the physical condition of the subjects: Figure 6 demonstrates that the measured physiological parameters are not sensitive to the thickness of overlying tissue. On the other hand, skinfold values are highly correlated

with BMI and people with higher BMI have lower hemoglobin concentration (Figure 7). This correlation can be explained by following two conjectures. First of all, it has been shown that bone mineral density (BMD) is decreased in people with higher BMI (Reid 2008, Hsu et al. 2006), this decrease in BMD of bone marrow may reduce the measured absorption coefficient. As long as we are not considering bone mineral in our chromophores, this reduction is reflected in the measured hemoglobin and consequently make the THC and BMI correlated. Secondly, in a recent study (Bredella et al. 2013) the correlation between serum lipid levels and bone marrow fat is observed. BMI and serum lipids also have positive correlation (Wakabayashi 2004). It can be concluded that in subjects with higher BMI, the red marrow cellularity would be lower. As red marrow is metabolically more active than marrow fat and is expected to have higher blood supply. Therefore, a lower THC is expected in the subjects with lower red marrow cellularity.

In Figure 6, one can observe a positive correlation between BMI and oxygen saturation. Since tissue with lower cellularity is physiologically less active, the oxygen consumption will be lower therefore the oxygen saturation increases.

However, to validate these hypotheses we need measurements with more wavelengths to be able to calculate the fat and bone mineral concentration for each subject individually. Then, we can investigate the correlation between BMI and lipid or bone concentration.

The dependency of the parameters on the gender of subjects: Optical parameters (μ_a and $\mu_s{}'$) as well as THC and BFI do not show any dependency on the gender of subjects while oxygen saturation in females is lower than males ($\approx 2\%$, $P = 0.02$). This observation can be explained as the effect of BMI on oxygen saturation. In Figure 7, it is shown that subjects with higher BMI have higher oxygen saturation. On the other hand, males have higher BMI in comparison to females (Table 2). Since BMI can influence the saturation and genders are different in BMI, we should rule out the effect of BMI. We have performed this by fitting an LME in which has BMI in addition to the gender and location of the probe as fixed effect. The results demonstrate that gender does not have a significant difference in oxygen saturation and BMI is the dominant parameter.

The dependency of parameters on the age of the subjects: Although hematological malignancies are the most common cancer in children and adolescents, due to ethical concerns we did not measure on this group of subjects. The effect of aging on the composition of bone marrow is well studied (Griffith et al. 2013, Richards et al. 1988, Justesen et al. 2001). In this study, we have measured a narrow range of age (24-42) in order to avoid any significant dependency of measured parameters on age. The correlation plots also shows that the chosen range of age is tight enough to have no significant correlation between measured optical parameters and age.

Outlook to the future: This study aimed to characterize the optical and physiological properties of healthy bone marrow with the goal of applying diffuse optics to study hematological malignancies. In the future, regarding this goal, we will characterize the same tissue on a group of patients with a specific type of hematological malignancy. The distribution of measured parameters on the healthy tissue will be compared with the the distribution on the malignant tissue. It is also interesting to observe the effect of anti-angiogenic therapy on the measured parameters.

5. Conclusions

Since hematological malignancies affect the red bone marrow, we have sought to investigate a noninvasive optical technique for the manubrium as a site, rich of red bone marrow in the adults. For the first time, we have characterized the optical and hemodynamics properties of the manubrium in thirty-two healthy subjects using TRS and DCS. This study is the first step in the path of applying optics for the studies on bone marrow cancer. The distribution of optical and physiological parameters in the healthy bone marrow is demonstrated. Measuring the same parameters in the patients with hematological malignancies will illustrate the difference between distribution of measured parameters on the healthy and malignant marrow. It can be applied for screening purposes to detect subjects with high risk of hematological malignancies. We can also monitor to changes in optical and physiological parameters induced by anti-angiogenic therapies to predict the effect of treatment and personalize the therapy.

Acknowledgements

We wish to express our gratitude to Mireia Mora Porta and Mattia Squarcia for their support during the measurements. We thank Ilaria Bargiggia and Antonio Giovanni Pifferi for providing us with the absorption spectrum of bone mineral. The authors acknowledge funding by Fundació Cellex Barcelona, Marie Curie IRG (FP7, RTPAMON), Institute de Salud Carlos III (DOMMON), Ministerio de Economía y Competitividad (PHOTOSTROKE), Institució CERCA, Generalitat de Catalunya (DOCNEURO), European Regional Development Fund and LASERLAB-EUROPE III (BIOPTHICAL) .

Disclosures

We disclose the following current or potential financial relationships. TD is an inventor on a relevant patent. ICFO has equity ownership in the spin-off company HemoPhotonics. UMW is the CEO and has equity ownership in HemoPhotonics. Potential financial conflicts of interest and objectivity of research have been monitored by ICFO's Knowledge & Technology Transfer Department.

Appendix A.

In the following tables the measured optical and physiological parameters for each subject averaged over all locations are reported.

Table A1. Absorption coefficient (cm^{-1})

Subject	$\lambda = 690$ nm	$\lambda = 785$ nm	$\lambda = 830$ nm
01	0.10 ± 0.00	0.11 ± 0.00	0.12 ± 0.00
02	0.15 ± 0.01	0.15 ± 0.01	0.16 ± 0.01
03	0.10 ± 0.00	0.10 ± 0.01	0.10 ± 0.01
04	0.08 ± 0.01	0.09 ± 0.01	0.10 ± 0.01
05	0.17 ± 0.00	0.16 ± 0.01	0.17 ± 0.01
06	0.14 ± 0.01	0.15 ± 0.01	0.16 ± 0.01
07	0.12 ± 0.01	0.12 ± 0.01	0.12 ± 0.01
08	0.09 ± 0.01	0.09 ± 0.01	0.10 ± 0.01
09	0.13 ± 0.00	0.13 ± 0.00	0.14 ± 0.00
10	0.15 ± 0.00	0.16 ± 0.00	0.17 ± 0.00
11	0.12 ± 0.01	0.14 ± 0.01	0.15 ± 0.01
12	0.14 ± 0.02	0.15 ± 0.02	0.16 ± 0.02
13	0.10 ± 0.01	0.11 ± 0.01	0.12 ± 0.01
14	0.16 ± 0.02	0.17 ± 0.02	0.17 ± 0.02
15	0.19 ± 0.02	0.19 ± 0.02	0.19 ± 0.02
16	0.13 ± 0.01	0.15 ± 0.01	0.16 ± 0.01
17	0.21 ± 0.03	0.20 ± 0.02	0.21 ± 0.02
18	0.18 ± 0.01	0.18 ± 0.01	0.20 ± 0.01
19	0.17 ± 0.01	0.17 ± 0.01	0.18 ± 0.01
20	0.17 ± 0.00	0.19 ± 0.00	0.20 ± 0.00
21	0.11 ± 0.00	0.12 ± 0.00	0.13 ± 0.00
22	0.22 ± 0.02	0.22 ± 0.01	0.24 ± 0.02
23	0.05 ± 0.01	0.06 ± 0.01	0.06 ± 0.01
24	0.14 ± 0.01	0.15 ± 0.01	0.16 ± 0.01
25	0.15 ± 0.02	0.16 ± 0.02	0.18 ± 0.02
26	0.12 ± 0.02	0.12 ± 0.02	0.14 ± 0.02
27	0.20 ± 0.01	0.19 ± 0.01	0.21 ± 0.02
28	0.13 ± 0.01	0.14 ± 0.01	0.15 ± 0.01
29	0.17 ± 0.01	0.17 ± 0.01	0.18 ± 0.01
30	0.11 ± 0.00	0.12 ± 0.00	0.13 ± 0.00
31	0.16 ± 0.02	0.17 ± 0.03	0.18 ± 0.03
32	0.12 ± 0.00	0.14 ± 0.00	0.15 ± 0.00

Table A2. Reduced scattering coefficient (cm^{-1})

Subject	λ = 690 nm	λ = 785 nm	λ = 830 nm
01	10.1 ± 0.4	09.5 ± 0.3	08.9 ± 0.4
02	11.4 ± 0.3	10.4 ± 0.2	09.3 ± 0.2
03	10.4 ± 0.7	09.9 ± 0.7	09.2 ± 0.6
04	09.6 ± 0.9	09.3 ± 0.9	08.6 ± 0.9
05	10.8 ± 1.0	10.2 ± 0.8	09.3 ± 0.7
06	10.1 ± 1.1	09.7 ± 1.0	08.8 ± 0.9
07	11.0 ± 1.2	10.6 ± 1.1	09.9 ± 1.0
08*	09.3 ± 0.3	08.9 ± 0.2	08.2 ± 0.2
09	09.8 ± 0.3	09.0 ± 0.3	08.3 ± 0.3
10	10.0 ± 0.8	09.3 ± 0.7	08.5 ± 0.7
11	09.7 ± 0.6	09.0 ± 0.5	08.3 ± 0.5
12	10.4 ± 0.7	09.6 ± 0.7	08.6 ± 0.6
13	09.9 ± 0.1	09.2 ± 0.2	08.5 ± 0.2
14	13.2 ± 0.4	12.6 ± 0.3	11.2 ± 0.3
15*	12.1 ± 0.4	11.5 ± 0.3	10.1 ± 0.3
16	09.7 ± 0.3	08.9 ± 0.3	08.3 ± 0.3
17	11.0 ± 0.3	10.1 ± 0.2	09.2 ± 0.3
18*	11.1 ± 0.4	10.2 ± 0.6	09.0 ± 0.5
19	12.1 ± 0.4	11.5 ± 0.4	10.2 ± 0.4
20	10.7 ± 0.2	10.3 ± 0.2	09.5 ± 0.2
21	10.3 ± 0.2	09.6 ± 0.2	08.9 ± 0.2
22	10.2 ± 0.5	09.2 ± 0.7	08.4 ± 0.5
23	09.5 ± 0.2	08.7 ± 0.2	08.1 ± 0.2
24	09.4 ± 0.5	08.9 ± 0.5	08.1 ± 0.4
25	11.3 ± 0.9	10.3 ± 0.8	09.4 ± 0.7
26	11.1 ± 0.4	10.1 ± 0.4	09.6 ± 0.3
27	09.8 ± 1.6	09.0 ± 0.6	08.4 ± 0.6
28	09.0 ± 0.5	08.3 ± 0.5	07.9 ± 0.5
29	10.2 ± 0.6	09.1 ± 0.5	08.3 ± 0.4
30	09.5 ± 0.2	08.8 ± 0.1	08.2 ± 0.1
31	10.8 ± 0.6	10.2 ± 0.5	09.0 ± 0.6
32	09.7 ± 0.3	09.4 ± 0.3	08.3 ± 0.3

* Smoker subjects.

Table A3. Physiological parameters

Subject	Blood flow index (cm^2/s)	Blood volume	Oxygen saturation (%)
01	$4.4\times10^{-9} \pm 1.6\times10^{-9}$	56.0 ± 1.4	71.4 ± 2.1
02	$4.0\times10^{-9} \pm 3.7\times10^{-10}$	77.3 ± 5.8	69.8 ± 0.9
03	$3.5\times10^{-9} \pm 6.2\times10^{-10}$	50.0 ± 3.1	68.5 ± 1.8
04	$7.4\times10^{-9} \pm 2.0\times10^{-9}$	48.4 ± 5.6	73.6 ± 1.2
05	$6.5\times10^{-9} \pm 2.6\times10^{-9}$	82.1 ± 5.4	65.2 ± 3.3
06	$5.6\times10^{-9} \pm 1.4\times10^{-9}$	78.7 ± 3.3	71.0 ± 1.1
07	$3.5\times10^{-9} \pm 1.0\times10^{-9}$	60.6 ± 3.9	69.4 ± 1.4
08*	$2.7\times10^{-9} \pm 6.3\times10^{-10}$	46.7 ± 4.8	68.5 ± 1.8
09	$3.7\times10^{-9} \pm 1.2\times10^{-9}$	70.1 ± 1.8	70.5 ± 1.0
10	$6.5\times10^{-9} \pm 2.9\times10^{-9}$	83.6 ± 2.1	71.7 ± 0.7
11	$4.5\times10^{-9} \pm 1.1\times10^{-9}$	73.2 ± 6.6	75.0 ± 0.5
12	$7.3\times10^{-9} \pm 3.0\times10^{-9}$	79.8 ± 10.5	71.8 ± 1.2
13	$5.1\times10^{-9} \pm 1.0\times10^{-9}$	55.5 ± 5.7	71.9 ± 1.1
14	$7.5\times10^{-9} \pm 2.4\times10^{-9}$	85.8 ± 9.3	70.6 ± 0.6
15*	$2.9\times10^{-9} \pm 5.3\times10^{-10}$	95.3 ± 11.4	67.8 ± 0.8
16	$8.7\times10^{-9} \pm 2.6\times10^{-9}$	77.2 ± 5.3	73.3 ± 0.6
17	$4.8\times10^{-9} \pm 1.1\times10^{-9}$	103.7 ± 12.1	65.9 ± 1.7
18*	$1.0\times10^{-8} \pm 5.3\times10^{-9}$	95.9 ± 4.0	70.1 ± 2.1
19	$4.3\times10^{-9} \pm 6.9\times10^{-10}$	88.8 ± 4.8	68.8 ± 1.1
20	$8.2\times10^{-9} \pm 2.2\times10^{-9}$	98.1 ± 1.8	72.6 ± 0.8
21	$4.7\times10^{-9} \pm 1.0\times10^{-9}$	61.1 ± 1.0	73.4 ± 0.9
22	$5.2\times10^{-9} \pm 1.5\times10^{-9}$	115.4 ± 6.3	70.1 ± 2.7
23	$9.7\times10^{-9} \pm 3.1\times10^{-9}$	29.6 ± 3.0	76.9 ± 1.3
24	$5.8\times10^{-9} \pm 1.9\times10^{-9}$	77.3 ± 6.1	72.1 ± 1.3
25	$9.2\times10^{-9} \pm 1.7\times10^{-9}$	86.5 ± 9.2	74.1 ± 1.0
26	$3.8\times10^{-9} \pm 1.1\times10^{-9}$	66.0 ± 9.2	71.8 ± 1.1
27	$8.4\times10^{-9} \pm 1.7\times10^{-9}$	101.0 ± 6.7	68.4 ± 2.3
28	$4.9\times10^{-9} \pm 2.0\times10^{-9}$	71.4 ± 4.3	70.8 ± 0.5
29	$6.0\times10^{-9} \pm 1.5\times10^{-9}$	90.0 ± 5.9	69.5 ± 1.0
30	$4.1\times10^{-9} \pm 1.4\times10^{-9}$	63.4 ± 2.4	71.9 ± 0.6
31	$4.8\times10^{-9} \pm 1.2\times10^{-9}$	88.4 ± 14.6	71.2 ± 1.4
32	$4.6\times10^{-9} \pm 1.6\times10^{-9}$	70.6 ± 1.9	73.2 ± 1.4

* Smoker subjects.

References

Alexandrakis M G, Passam F H, Dambaki C, Pappa C a & Stathopoulos E N 2004 The relation between bone marrow angiogenesis and the proliferation index Ki-67 in multiple myeloma. *Journal of clinical pathology* **57**(8), 856–60.

Arbabi A 2009 A quantitative analysis of the structure of human sternum. *Journal of medical physics* **34**(2), 80–6.

Aziz S M, Khambatta F, Vaithianathan T, Thomas J C, Clark J M & Marshall R 2010 A near infrared instrument to monitor relative hemoglobin concentrations of human bone tissue in vitro and in vivo. *The Review of scientific instruments* **81**(4), 043111.

Bashkatov A N 2006 Optical properties of human cranial bone in the spectral range from 800 to 2000 nm *Proceedings of SPIE* **6163**, 616310–616310–11.

Bates D, Maechler M, Bolker B & Walker S 2013 *lme4: Linear mixed-effects models using Eigen and S4*.

Beer A J & Schwaiger M 2008 Imaging of integrin alphavbeta3 expression. *Cancer metastasis reviews* **27**(4), 631–44.

Bertolini F, Mancuso P, Shaked Y & Kerbel R S 2007 Molecular and cellular biomarkers for angiogenesis in clinical oncology. *Drug discovery today* **12**(19-20), 806–12.

Bhatti S S, Kumar L, Dinda A K & Dawar R 2006 Prognostic value of bone marrow angiogenesis in multiple myeloma: use of light microscopy as well as computerized image analyzer in the assessment of microvessel density and total vascular area in multiple myeloma and its correlation with various clinical *American journal of hematology* **81**(9), 649–56.

Bhutani M, Turkbey B, Tan E, Kemp T J, Pinto L a, Berg a R, Korde N, Minter a R, Weiss B M, Mena E, Lindenberg L, Aras O, Purdue M P, Hofmann J N, Steinberg S M, Calvo K R, Choyke P L, Maric I, Kurdziel K & Landgren O 2013 Bone marrow angiogenesis in myeloma and its precursor disease: a prospective clinical trial. *Leukemia* (September), 1–4.

Binzoni T, Bianchi S, Fasel J H, Bounameaux H, Hiltbrand E & Delpy D 2002 Human tibia bone marrow blood perfusion by non-invasive near infrared spectroscopy: a new tool for studies on microgravity *Life in space for life on earth* **501**, 103–104.

Binzoni T, Boggett D & Van De Ville D 2011 Laser-Doppler flowmetry at large interoptode spacing in human tibia diaphysis: Monte Carlo simulations and preliminary experimental results *Physiological Measurement* **32**, N33.

Binzoni T, Leung T, Hollis V, Bianchi S, Fasel J H D, Bounameaux H, Hiltbrand E & Delpy D 2003 Human tibia bone marrow: defining a model for the study of haemodynamics as a function of age by near infrared spectroscopy. *Journal of physiological anthropology and applied human science* **22**(5), 211–8.

Binzoni T, Leung T S, Courvoisier C, Giust R, Tribillon G, Gharbi T & Delpy D T 2006 Blood Volume and Haemoglobin Oxygen Content Changes in Human Bone Marrow during Orthostatic Stress *Journal of physiological anthropology* **25**(1), 1–6.

Binzoni T, Tchernin D, Hyacinthe J N, Van De Ville D & Richiardi J 2013 Pulsatile blood flow in human bone assessed by laser-Doppler flowmetry and the interpretation of photoplethysmographic signals. *Physiological measurement* **34**(3), N25–40.

Binzoni T & Van De Ville D 2011 Noninvasive Probing of the Neurovascular System in Human Bone/Bone Marrow Using Near-Infrared Light *Journal of Innovative optical health sciences* **04**(02), 183.

Boas D, Campbell L & Yodh A 1995 Scattering and Imaging with Diffusing Temporal Field Correlations *Physical Review Letters* **75**(9), 1855–1858.

Bredella M A, Gill C M, Gerweck A V, Landa M G, Kumar V, Daley S M, Torriani M & Miller K K 2013 Ectopic and serum lipid levels are positively associated with bone marrow fat in obesity. *Radiology* **269**(2), 534–41.

De Raeve H, Van Marck E, Van Camp B & Vanderkerken K 2004 Angiogenesis and the role of

bone marrow endothelial cells in haematological malignancies. *Histology and histopathology* **19**(3), 935–50.

Durduran T, Choe R, Baker W B & Yodh A G 2010 Diffuse optics for tissue monitoring and tomography *Reports on Progress in Physics* **73**(7), 076701.

Durduran T, Choe R, Yu G, Zhou C, Tchou J C, Czerniecki B J & Yodh A G 2005 Diffuse optical measurement of blood flow in breast tumors. *Optics letters* **30**(21), 2915–7.

Durduran T & Yodh A G 2014 Diffuse correlation spectroscopy for non-invasive, micro-vascular cerebral blood flow measurement. *NeuroImage* **85 Pt 1**, 51–63.

Farzam P, Zirak P, Binzoni T & Durduran T 2013 Pulsatile and steady-state hemodynamics of the human patella bone by diffuse optical spectroscopy. *Physiological measurement* **34**(8), 839–57.

Firbank M, Hiraoka M, Essenpreis M & Delpy D T 1993 in the wavelength range 650-950 nm *Physics in medicine and biology* **38**, 503.

Gao-ju W & Qing W 2011 Feasibility of manubrium sterni cancellous bone plus pyramesh in anterior cervical spinal fusion surgery *Journal of Clinical Rehabilitative Tissue Engineering Research* **15**(9), 1698–1701.

Gerber H P & Ferrara N 2003 The role of VEGF in normal and neoplastic hematopoiesis. *Journal of molecular medicine (Berlin, Germany)* **81**(1), 20–31.

Gordon M Y, Douglas I D, Clink H M & Pickering B M 1976 Distribution of granulopoietic activity in the human skeleton, studied by colony growth in agar diffusion chambers. *British journal of haematology* **32**(4), 537–42.

Greenberg P, Cox C, LeBeau M M, Fenaux P, Morel P, Sanz G, Sanz M, Vallespi T, Hamblin T, Oscier D, Ohyashiki K, Toyama K, Aul C, Mufti G & Bennett J 1997 International scoring system for evaluating prognosis in myelodysplastic syndromes. *Blood* **89**(6), 2079–88.

Griffith J F, BAO B & Others 2013 *in* 'Geriatric Imaging' Springer pp. 891–904.

Griffith J F, Yeung D K W, Antonio G E, Lee F K H, Hong A W L, Wong S Y S, Lau E M C & Leung P C 2005 Vertebral bone mineral density, marrow perfusion, and fat content in healthy men and men with osteoporosis: dynamic contrast-enhanced MR imaging and MR spectroscopy. *Radiology* **236**(3), 945–51.

Horger M & Bares R 2006 The role of single-photon emission computed tomography/computed tomography in benign and malignant bone disease. *Seminars in nuclear medicine* **36**(4), 286–94.

Hsu Y H, Venners S a, Terwedow H a, Feng Y, Niu T, Li Z, Laird N, Brain J D, Cummings S R, Bouxsein M L, Rosen C J & Xu X 2006 Relation of body composition, fat mass, and serum lipids to osteoporotic fractures and bone mineral density in Chinese men and women. *The American journal of clinical nutrition* **83**(1), 146–54.

Irwin D, Dong L, Shang Y, Cheng R, Kudrimoti M, Stevens S D & Yu G 2011 Influences of tissue absorption and scattering on diffuse correlation spectroscopy blood flow measurements. *Biomedical optics express* **2**(7), 1969–85.

Jelkmann W 2001 Pitfalls in the measurement of circulating vascular endothelial growth factor. *Clinical chemistry* **47**(4), 617–23.

Justesen J, Stenderup K, Ebbesen E N, Mosekilde L, Steiniche T & Kassem M 2001 Adipocyte tissue volume in bone marrow is increased with aging and in patients with osteoporosis *Biogerontology* **2**(3), 165–171.

Kahn D, Weiner G J, Ben-Haim S, Ponto L L, Madsen M T, Bushnell D L, Watkins G L, Argenyi E A & Hichwa R D 1994 Positron emission tomographic measurement of bone marrow blood flow to the pelvis and lumbar vertebrae in young normal adults. *Blood* **83**(4), 958–63.

Kini A R, Kay N E & Peterson L C 2000 Increased bone marrow angiogenesis in B cell chronic lymphocytic leukemia *Leukemia* **14**(8), 1414–1418.

Klasing M & Zange J 2003 In vivo quantitative near-infrared spectroscopy in skeletal muscle and bone during rest and isometric exercise *European conference on biomedical optics* **5138**(0), 318–322.

Kumar S, Gertz M A, Dispenzieri A, Lacy M Q, Wellik L A, Fonseca R, Lust J A, Witzig T E, Kyle R A, Greipp P R & Rajkumar S V 2004 Prognostic value of bone marrow angiogenesis

in patients with multiple myeloma undergoing high-dose therapy. *Bone marrow transplantation* **34**(3), 235–9.

Kuznetsova A, Bruun Brockhoff P & Haubo Bojesen Christensen R 2013 *lmerTest: Tests for random and fixed effects for linear mixed effect models (lmer objects of lme4 package).*

Li W W, Hutnik M & Gehr G 2008 Antiangiogenesis in haematological malignancies. *British journal of haematology* **143**(5), 622–31.

Malcovati L, Germing U, Kuendgen A, Della Porta M G, Pascutto C, Invernizzi R, Giagounidis A, Hildebrandt B, Bernasconi P, Knipp S, Strupp C, Lazzarino M, Aul C & Cazzola M 2007 Time-dependent prognostic scoring system for predicting survival and leukemic evolution in myelodysplastic syndromes. *Journal of clinical oncology : official journal of the American Society of Clinical Oncology* **25**(23), 3503–10.

Mangi M H & Newland A C 2000 Angiogenesis and angiogenic mediators in haematological malignancies *British Journal of Haematology* **111**(1), 43–51.

Mateus J & Hargens A R 2012 Photoplethysmography for non-invasive in vivo measurement of bone hemodynamics *Physiological Measurement* **33**(6), 1027.

Mateus J & Hargens A R 2013 Bone hemodynamic responses to changes in external pressure *Bone* **52**(2), 604–610.

McCarthy I 2006 The physiology of bone blood flow: a review. *The Journal of bone and joint surgery. American volume* **88 Suppl 3**(suppl_2), 4–9.

Mesquita R C, Durduran T, Yu G, Buckley E M, Kim M N, Zhou C, Choe R, Sunar U & Yodh A G 2011 Direct measurement of tissue blood flow and metabolism with diffuse optics. *Philosophical transactions. Series A, Mathematical, physical, and engineering sciences* **369**(1955), 4390–406.

Mesquita R C, Schenkel S S, Minkoff D L, Lu X, Favilla C G, Vora P M, Busch D R, Chandra M, Greenberg J H, Detre J a & Yodh a G 2013 Influence of probe pressure on the diffuse correlation spectroscopy blood flow signal: extra-cerebral contributions *Biomedical Optics Express* **4**(7), 978.

Mesquita R C, Skuli N, Kim M N, Liang J, Schenkel S, Majmundar A J, Simon M C & Yodh A G 2010 Hemodynamic and metabolic diffuse optical monitoring in a mouse model of hindlimb ischemia. *Biomedical optics express* **1**(4), 1173–1187.

Molica S, Vacca A, Ribatti D, Cuneo A, Cavazzini F, Levato D, Vitelli G, Tucci L, Roccaro A M & Dammacco F 2002 Prognostic value of enhanced bone marrow angiogenesis in early B-cell chronic lymphocytic leukemia. *Blood* **100**(9), 3344–51.

Näslund J E, Näslund S, Lundeberg E, Lindberg L G & Lund I 2011 Bone blood flow is influenced by muscle contractions *Journal of biomedical science and engineering* **04**(07), 490–496.

Näslund J, Pettersson J, Lundeberg T, Linnarsson D & Lindberg L G 2006 Non-invasive continuous estimation of blood flow changes in human patellar bone. *Medical & biological engineering & computing* **44**(6), 501–9.

Näslund J, Waldén M & Lindberg L G 2007 Decreased pulsatile blood flow in the patella in patellofemoral pain syndrome. *The American journal of sports medicine* **35**(10), 1668–73.

Negaard H F S, Iversen N, Bowitz-Lothe I M, Sandset P M, Steinsvik B, Ostenstad B & Iversen P O 2009 Increased bone marrow microvascular density in haematological malignancies is associated with differential regulation of angiogenic factors. *Leukemia* **23**(1), 162–9.

Ntziachristos V, Ma X, Yodh a G & Chance B 1999 Multichannel photon counting instrument for spatially resolved near infrared spectroscopy *Review of Scientific Instruments* **70**(1), 193.

Ntziachristos V, Yodh a G, Schnall M D & Chance B 2002 MRI-guided diffuse optical spectroscopy of malignant and benign breast lesions. *Neoplasia (New York, N.Y.)* **4**(4), 347–54.

Padró T, Ruiz S, Bieker R, Bürger H, Steins M, Kienast J, Büchner T, Berdel W E & Mesters R M 2000 Increased angiogenesis in the bone marrow of patients with acute myeloid leukemia. *Blood* **95**(8), 2637–44.

Pakalniskis M G, Wells W A, Schwab M C, Froehlich H M, Jiang S, Li Z, Tosteson T D, Poplack S P, Kaufman P A, Pogue B W & Paulsen K D 2011 Tumor angiogenesis change estimated by using diffuse optical spectroscopic tomography: demonstrated correlation in women undergoing

neoadjuvant chemotherapy for invasive breast cancer? *Radiology* **259**(2), 365–74.

Patterson M, Chance B & Wilson B 1989 Time resolved reflectance and transmittance for the non-invasive measurement of tissue optical properties *Appl. Opt* **28**(12), 2331–2336.

Pifferi A, Torricelli A, Taroni P, Bassi A, Chikoidze E, Giambattistelli E & Cubeddu R 2004 Optical biopsy of bone tissue: a step toward the diagnosis of bone pathologies. *Journal of biomedical optics* **9**(3), 474–80.

Pinheiro J C & Bates D M 2000 *Mixed-effects models in S and S-PLUS* Springer Verlag New York.

Prahl S n.d. Optical absorption of hemoglobin *http://omlc.ogi.edu/spectra. Accessed 2013* .

Prapavat V, Runge W, Mans J, Krause A, Beuthan J & Müller G 1997 The development of a finger joint phantom for the optical simulation of early inflammatory rheumatic changes. *Biomedizinische Technik. Biomedical engineering* **42**(11), 319.

R Core Team 2013 *R: A Language and Environment for Statistical Computing* R Foundation for Statistical Computing Vienna, Austria.

Rajkumar S V, Mesa R A & Tefferi A 2002 A review of angiogenesis and anti-angiogenic therapy in hematologic malignancies. *Journal of hematotherapy & stem cell research* **11**(1), 33–47.

Reid I R 2008 Relationships between fat and bone. *Osteoporosis international : a journal established as result of cooperation between the European Foundation for Osteoporosis and the National Osteoporosis Foundation of the USA* **19**(5), 595–606.

Richards M A, Webb J A, Jewell S E, Gregory W M & Reznek R H 1988 In-vivo measurement of spin lattice relaxation time (T1) of bone marrow in healthy volunteers: the effects of age and sex. *The British journal of radiology* **61**, 30–33.

Rodriguez-Abreu D, Bordoni A & Zucca E 2007 Epidemiology of hematological malignancies. *Annals of oncology : official journal of the European Society for Medical Oncology / ESMO* **18 Suppl 1**(Supplement 1), i3–i8.

Salven P, Orpana A, Teerenhovi L & Joensuu H 2000 Simultaneous elevation in the serum concentrations of the angiogenic growth factors VEGF and bFGF is an independent predictor of poor prognosis in non-Hodgkin lymphoma: a single-institution study of 200 patients. *Blood* **96**(12), 3712–8.

Sant M, Allemani C, Tereanu C, De Angelis R, Capocaccia R, Visser O, Marcos-Gragera R, Maynadié M, Simonetti A, Lutz J M & Berrino F 2010 Incidence of hematologic malignancies in Europe by morphologic subtype: results of the HAEMACARE project. *Blood* **116**(19), 3724–34.

Selthofer R, Nikolić V, Mrcela T, Radić R, Leksan I, Rudez I & Selthofer K 2006 Morphometric analysis of the sternum. *Collegium antropologicum* **30**(1), 43–7.

Sezer O, Niemöller K, Kaufmann O, Eucker J, Jakob C, Zavrski I & Possinger K 2001 Decrease of bone marrow angiogenesis in myeloma patients achieving a remission after chemotherapy. *European journal of haematology* **66**(4), 238–44.

Shinkaruk S, Bayle M, Laïn G & Déléris G 2003 Vascular endothelial cell growth factor (VEGF), an emerging target for cancer chemotherapy. *Current medicinal chemistry. Anti-cancer agents* **3**(2), 95–117.

Svensson T, Andersson-Engels S, Einarsdóttír M & Svanberg K 2007 In vivo optical characterization of human prostate tissue using near-infrared time-resolved spectroscopy. *Journal of biomedical optics* **12**(1), 014022.

Taroni P, Pifferi A, Quarto G, Spinelli L, Torricelli A, Abbate F, Villa A, Balestreri N, Menna S, Cassano E & Cubeddu R 2010 Noninvasive assessment of breast cancer risk using time-resolved diffuse optical spectroscopy. *Journal of biomedical optics* **15**(6), 060501.

Torricelli A, Contini D, Pifferi A, Caffini M, Re R, Zucchelli L & Spinelli L 2013 Time domain functional NIRS imaging for human brain mapping. *NeuroImage* .

Ugryumova N, Matcher S J & Attenburrow D P 2004 Measurement of bone mineral density via light scattering *Physics in medicine and biology* **49**, 469.

Vacca A, Ribatti D, Roncali L, Ranieri G, Serio G, Silvestris F & Dammacco F 1994 Bone marrow angiogenesis and progression in multiple myeloma. *British journal of haematology* **87**(3), 503–8.

Van Veen R L P, Sterenborg H & van Veen R 2004 Determination of VIS-NIR absorption coefficients

of mammalian fat, with time-and spatially resolved diffuse reflectance and transmission spectroscopy *Biomedical Topical Meeting, OSA Technical Digest* pp. 1–3.

Wakabayashi I 2004 Relationships of body mass index with blood pressure and serum cholesterol concentrations at different ages. *Aging clinical and experimental research* **16**(6), 461–6.

White D R, Woodard H Q & Hammond S M 1987 Average soft-tissue and bone models for use in radiation dosimetry. *The British journal of radiology* **60**(717), 907–13.

Winter B 2013 Linear models and linear mixed effects models in R with linguistic applications p. 42.

Wolowiec D, Wozniak Z, Potoczek S, Ganczarski G, Wrobel T, Kuliczkowski K, Frydecka I & Jele M 2004 Bone marrow angiogenesis and proliferation in B-cell chronic lymphocytic leukemia. *Analytical and quantitative cytology and histology / the International Academy of Cytology [and] American Society of Cytology* **26**(5), 263–70.

Xiu P, Shui D, Wang Q, Wang G & Lan Y 2012 Anatomic and morphometric analysis of manubrium sterni as a source of autograft for anterior cervical fusion surgery using quantitative 3-dimensional computed tomographic scans. *Spine* **37**(16), E935–41.

Xu Y, Iftimia N, Jiang H, Key L & Bolster M 2001 Imaging of in vitro and in vivo bones and joints with continuous-wave diffuse optical tomography. *Optics express* **8**(7), 447–51.

Yu G 2012 Near-infrared diffuse correlation spectroscopy in cancer diagnosis and therapy monitoring. *Journal of biomedical optics* **17**(1), 010901.

Zangar R C, Daly D S & White A M 2006 ELISA microarray technology as a high-throughput system for cancer biomarker validation. *Expert review of proteomics* **3**(1), 37–44.

Zhang Q & Jiang H 2005 Three-dimensional diffuse optical imaging of hand joints: System description and phantom studies *Optics and Lasers in Engineering* **43**(11), 1237–1251.